The Spine Journal 22 (2022) 1742–1757

Basic Science

Outstanding *in vivo* mechanical integrity of additively manufactured spinal cages with a novel "honeycomb tree structure" design via guiding bone matrix orientation

Takuya Ishimoto, PhD[a,b], Yoshiya Kobayashi, MEng[a], Masahiko Takahata, MD, PhD[c], Manabu Ito, MD, PhD[d], Aira Matsugaki, PhD[a,b], Hiroyuki Takahashi, PhD[a,e], Ryota Watanabe, MEng[a,e], Takayuki Inoue, PhD[e], Tadaaki Matsuzaka, MEng[a], Ryosuke Ozasa, PhD[a,b], Takao Hanawa, PhD[a,f], Katsuhiko Yokota, BA[e], Yoshio Nakashima, MEng[e], Takayoshi Nakano, PhD[a,b,*]

[a] *Division of Materials and Manufacturing Science, Graduate School of Engineering, Osaka University, 2-1, Yamada-Oka, Suita, Osaka, 565-0871, Japan*

[b] *Anisotropic Design and Additive Manufacturing Research Center, Osaka University, 2-1 Yamada-Oka, Suita, Osaka, 565-0871, Japan*

[c] *Department of Orthopedic Surgery, Graduate School of Medicine, Hokkaido University, North-15, West-7, Kita-ku, Sapporo, Hokkaido, 060-8638, Japan*

[d] *Department of Spine and Spinal Cord Disorders, National Hospital Organization, Hokkaido Medical Center, 5-7-1-1, Yamanote, Nishi-ku, Sapporo, Hokkaido, 063-0005, Japan*

[e] *Teijin Nakashima Medical Co., Ltd., 688-1 Joto-Kitagata, Higashi-ku, Okayama, 709-0625, Japan*

[f] *Institute of Biomaterials and Bioengineering, Tokyo Medical and Dental University, 2-3-10 Kanda-Surugadai, Chiyoda-ku, Tokyo, 101-0062, Japan*

Received 19 January 2022; revised 31 May 2022; accepted 31 May 2022

Abstract

BACKGROUND CONTEXT: Therapeutic devices for spinal disorders, such as spinal fusion cages, must be able to facilitate the maintenance and rapid recovery of spinal function. Therefore, it would be advantageous that future spinal fusion cages facilitate rapid recovery of spinal function without secondary surgery to harvest autologous bone.

PURPOSE: This study investigated a novel spinal cage configuration that achieves *in vivo* mechanical integrity as a devise/bone complex by inducing bone that mimicked the sound trabecular bone, hierarchically and anisotropically structured trabeculae strengthened with a preferentially oriented extracellular matrix.

STUDY DESIGN/SETTINGS: *In vivo* animal study.

METHODS: A cage possessing an anisotropic through-pore with a grooved substrate, that we termed "honeycomb tree structure," was designed for guiding bone matrix orientation; it was manufactured using a laser beam powder bed fusion method through an additive manufacturing processes. The newly designed cages were implanted into sheep vertebral bodies for 8 and 16 weeks. An autologous bone was not installed in the newly designed cage. A pull-out test was performed to evaluate the mechanical integrity of the cage/bone interface. Additionally, the preferential orientation of bone matrix consisting of collagen and apatite was determined.

FDA device/drug status: Not applicable.

Author disclosures: ***AM:*** Nothing to disclose. ***HT***: Nothing to disclose. ***KY***: Nothing to disclose. ***MI***: Nothing to disclose. ***MT***: Nothing to disclose. ***RO***: Nothing to disclose. ***RW***: Nothing to disclose. ***TM***: Nothing to disclose. ***TH***: Nothing to disclose. ***TN***: Grants: JSPS (H, Paid directly to institution); AMED (F, Paid directly to institution). ***TI***: Nothing to disclose. ***TI***: Nothing to disclose. ***YN***: Nothing to disclose. ***YK***: Nothing to disclose.

*Corresponding author. Division of Materials and Manufacturing Science, Graduate School of Engineering, Osaka University, 2-1, Yamada-Oka, Suita, Osaka, 565-0871, Japan. Tel/fax: (81) 6-6879-7505.

E-mail address: nakano@mat.eng.osaka-u.ac.jp (T. Nakano).

https://doi.org/10.1016/j.spinee.2022.05.006

RESULTS: The cage/host bone interface strength assessed by the maximum pull-out load for the novel cage without an autologous bone graft (3360±411 N) was significantly higher than that for the conventional cage using autologous bone (903±188 N) after only 8 weeks post-implantation.
CONCLUSIONS: These results highlight the potential of this novel cage to achieve functional fusion between the cage and host bone. Our study provides insight into the design of highly functional spinal devices based on the anisotropic nature of bone.
CLINICAL SIGNIFICANCE: The sheep spine is similar to the human spine in its stress condition and trabecular bone architecture and is widely recognized as a useful model for the human spine. The present design may be useful as a new spinal device for humans.

Keywords: Anisotropy; Bone quality; Bone matrix; Collagen/apatite orientation; Pull-out strength; Spinal cage; Trabecular architecture

Introduction

The spine plays critical functional roles including load-bearing and hematopoiesis. As such, therapeutic devices for spinal disorders, such as spinal fusion cages, must be able to facilitate the maintenance and rapid recovery of spinal function. In addition, minimally invasive spine fusion has become increasingly important [1] to reduce blood loss, shorten hospital stays, and promote the resumption of social activities. Therefore, it is imperative that future spinal fusion cages facilitate rapid recovery of spinal function.

The properties of osteogenicity, osteoinductivity, and osteoconductivity are crucial biological factors for achieving spinal fusion. Autologous iliac crest bone grafts are typically used as the gold-standard methodology to introduce osteogenicity, osteoinductivity, and osteoconductivity [2]. Autologous bone grafts mitigate the risk of immunogenic reactions and disease transmission. Nevertheless, the need for a secondary operation to harvest autologous bone, postoperative pain, and limited graft availability are major disadvantages that impose a physical and mental burden on patients.

Bone mechanical functions are not determined solely by bone mass and bone density; the preferential orientation of bone extracellular matrix (ECM), which is predominantly composed of collagen and apatite [3] also contributes significantly to bone strength [4−6]. Collagen [7] and apatite [8] both exhibit anisotropic mechanical properties, and the directions for greater strength (fiber axis for collagen and *c*-axis for apatite) are co-oriented due to *in vivo* self-assembly [3]. Therefore, the mechanical anisotropy of bone is enhanced by the formation of collagen/apatite complexes. Due to the inherent properties of bone, the direction of strength of the collagen/apatite complex is preferentially oriented in the principal direction of mechanical loading [9], and the strength of bone is enhanced in the preferential orientation direction of collagen/apatite [4−6]. This indicates that the direction and degree of preferential orientation of collagen/apatite may modulate bone strength without concomitant changes in bone mass and density.

The spine is characterized by abundant trabecular bone in the vertebral bodies. Vertebral trabeculae show an anisotropic macro-architecture defined by trabeculae predominantly running parallel to the cephalocaudal axis [10], where the principal stresses are applied. Furthermore, at the nanometer scale, collagen fibers and crystalline apatite *c*-axis preferentially orient along a trabecular long axis [10,11]. Therefore, vertebral trabecular bone shows a hierarchical and anisotropic structure where trabeculae are strengthened with a preferentially oriented ECM within the principally loaded cephalocaudal axis [10,11].

For bone defect regeneration, which resembles bone reactions immediately after cage implantation, ECM orientation has yet to be established, and the regenerated bone exhibits immature mechanical properties even if bone mass and density are fully restored. Recovery of ECM orientation occurs over a longer period than that of bone density [6]. This results in increased bone strength without an increase in bone density in the latter stage of bone regeneration [6,12−14]. Possible causes of non-oriented ECM formation in the early stages of bone regeneration include (1) the absence of mechanical stress and (2) excessive osteogenic activity accompanied by dysfunctional osteoblast activity and high bone formation rate due to recruitment of cytokines and stem cells at the fracture site. Bone formation rate and degree of ECM orientation are inversely correlated [15], indicating that higher rates of bone formation are associated with more disordered ECM orientation. Further, the collective movement of osteoblasts during bone formation has been reported to determine the highly regulated nanoarrangement of the ECM [16].

Based on these findings, we derived a design strategy for a novel spinal fusion cage involving the induction of mechanically integrated bone tissue that would exhibit preferential ECM orientation along the principally loaded direction corresponding to the cephalocaudal axis and to preserve this structure over a long period. To this end, we introduced a specific structure into the cage to induce ECM orientation even without stress and to transmit stress through the newly formed bone in the cage and subsequently maintain the induced ECM orientation. Further, we

refrained from using autologous bone to avoid an excessive increase in osteogenic activity. It was assumed that there would be less bone formation around the cage without the use of autologous bone; however, we hypothesized that the induction of bone with ECM orientation in the principally loaded cephalocaudal axis (ie, high-quality bone) would mechanically compensate for this. Furthermore, the absence of autologous bone would circumvent the aforementioned disadvantages associated with autologous bone collection.

Surface topographical cues play a vital role in regulating morphology, adhesion, differentiation, migration, proliferation, and, ultimately, the fate of cells [17]. In particular, cells cultured on an anisotropic grooved substrate are elongated in parallel to the direction of the grooves [18,19], and the elongated cells (osteoblasts) secrete collagen fibers that align in parallel to the cell elongation axis [20,21]. Furthermore, apatite crystallizes on collagen such that its *c*-axis lies parallel to the collagen fiber axis [22], which induces the production of a natural bone-mimetic ECM *in vitro*. We hypothesized that an anisotropic grooved substrate would enable the induction of ECM-oriented bone that mimicked natural bone *in vivo*, and that anisotropic substrate micro-patterning would activate the mechanobiological response of osteoblasts which underpins collagen secretion.

To test this hypothesis, we prepared a 10-mm square plate-shaped grooved substrate for an osteoblast culture experiment. Appropriate selection of groove dimensions is required to achieve osteoblast alignment [23]. For devices with a three-dimensional structure, it is necessary to design groove dimensions within an achievable accuracy range. In this study, a laser beam powder bed fusion (PBF-LB) as an additive manufacturing technology, which enabled the production of highly accurate three-dimensional structures, was used for fabrication. See Supplementary Texts for details on fabrication methods. The micro-computed tomography (μCT) images for the general appearance of the substrates are shown in Supplementary Fig. 1S. Although unmelted powder particles were trapped on the substrate surface immediately after fabrication (Fig. 1A), the fine groove structure was exposed by acid washing (Fig. 1B and C).

According to the osteoblast culture experiment (see Supplementary Texts for details), osteoblasts preferentially align parallel to the groove direction (Fig. 1E1 and E2), while the cells show random directionality on the control substrate (Fig. 1D1 and D2). Moreover, on the grooved substrate, the osteoblast-secreted type-I collagen fibers tended to orient parallel to the cell-elongation direction (groove direction) (Fig. 1E3), whereas the collagen on the control substrate did not (Fig. 1D3). By incorporating this grooved substrate into the cage, new bone with an oriented ECM is expected to be induced in the cage.

In this study, our aim was to design a spinal fusion cage for bone induction with a normally oriented ECM around and inside of the cage without the use of autologous bone inside the cage, which has been introduced hitherto, into the design of the cage. To validate the usefulness of the newly developed design, sheep vertebrae, which are similar to human vertebrae in terms of stress conditions [24], shape [25], and trabecular architecture [24] and have been validated as human vertebral models [26], were used as hosts. The novel cage would provide a direct scaffold for bone formation with an ECM orientation, resulting in functional fusion between the cage and bone at an early stage.

Materials and methods

Cage design

A cylinder-shaped cage with a diameter and height of 10 mm and 20 mm, respectively, was designed whereby the grooved substrate was placed such that the groove directions were unidirectionally aligned (Fig. 2A and B). The grooved substrate was placed to form an equilateral triangle inscribed by a circle with a diameter of 1 mm (Fig. 2C and D). The spacing between the substrates (the diameter of the inscribed circle) was determined based on the trabecular architectural indices of the lumbar vertebral body, trabecular number of 1.5 to 2 mm^{-1}, trabecular thickness of 0.1 to 0.2 mm, and trabecular spacing of 0.3 to 0.6 mm [27–29], such that the original trabecular bone structure was approximately reproduced when bone formed on the substrate surface. We hypothesized that this concept would make it easier for the trabeculae inside and outside the cage to exhibit a continuous connection. Finally, the design of the main functional structure of the cage, comprising a through-pore with a grooved substrate that we termed a "honeycomb tree structure (HTS)," was determined. The structure was composed of solid walls on the sides, bottom, and top of the cage as well as holes on the sides and bottom walls to ensure fluid circulation between the inside and outside of the cage (Fig. 2A and B).

Fabrication of spinal cages

Three types of spinal cages comprising a cylindrical outer shape with a diameter of 10 mm and a height of 20 mm were modeled using CAD (Fig. 3, Supplementary Fig. 2S). Type_A was a control cage with a large space in the center, which was adapted to many conventional cages. The space dimensions were determined such that the projected area of the opening (white regions in Fig. 3A-C) was equivalent to that of type_B and type_C cages. Autologous bone collected from the iliac crest was introduced into the space. Type_B was a newly designed cage with HTS. Type_C had the same basic structure as Type_B but contained a longitudinal through-hole with a diameter of 3 mm in the center of the cylinder parallel to the height direction, which enabled the introduction of autologous bone. A screw hole was prepared in the top part of each cage to enable the performance of a pull-out test (Fig. 2B). Cages were produced from Ti-6Al-4V ELI powder (EOS, Krailling, Germany) using the PBF-LB system (M 290; EOS) according to the CAD model, and then

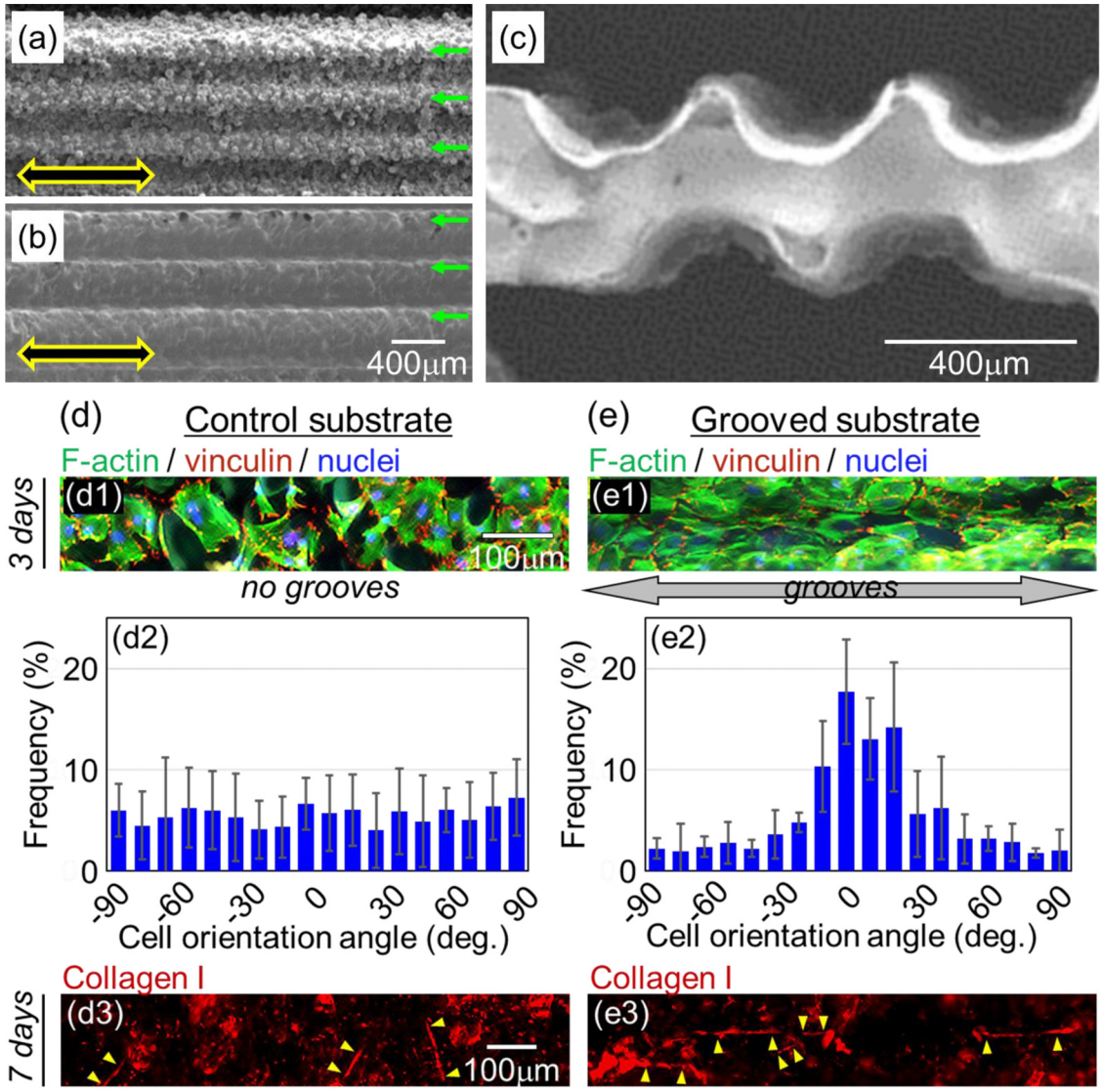

Fig. 1. Images of the produced substrate with unidirectionally elongated grooves for cell culture experiments and aligned osteoblasts and the secreted type-I collagen on the grooved substrate. Scanning electron microscopy (SEM) images of the substrate (A) before and (B) after washing with acid to remove trapped unmelted powder particles. The location of the ridge portion of the groove structure is indicated by green arrows. (C) SEM image of the top edge of the substrate indicative of the groove shape. Results of cell culture experiments for (D) the control substrate with no grooves and (E) grooved substrate; (D1, E1) fluorescence microscope image of osteoblasts cultured on the substrate; (D2, E2) quantified cell orientation distribution along the groove direction; and (D3, E3) cell-produced type-I collagen fibers. Arrow heads in (D3, E3) indicate collagen fiber direction. On the grooved substrate, well-aligned osteoblasts and collagen fibers parallel to the groove direction are represented.

washed with acid as described earlier. A cage with the designed shape was successfully produced (Fig. 2E and Supplementary Fig. 3S). The cages were sterilized using an autoclave.

Sheep model and surgical procedure

Experiments involving animals in this study were conducted in accordance with the Guidelines for Proper Conduct of Animal Experiments established by the Science Council of Japan. This study was approved by the Institutional Review Board of the Bioscience Department/Toya laboratory of Hokudo Co, Ltd. Eight adult male Suffolk sheep (16.5±6.2 months of age, weighing 55.6±6.3 kg) were used. Drill holes with a diameter of 9 mm were made laterally in the vertebral bodies of L1, L2, L3, and L4 using an electric drill. The cage was inserted using a right retroperitoneal approach (Supplementary Fig. 4Sa) under general anesthesia. Four experimental groups were prepared based on the cage type and implantation direction, as follows:

Group_A: Type_A cage with an autologous bone graft in the central open pore, implanted such that the pore penetrated the cephalocaudal axis.

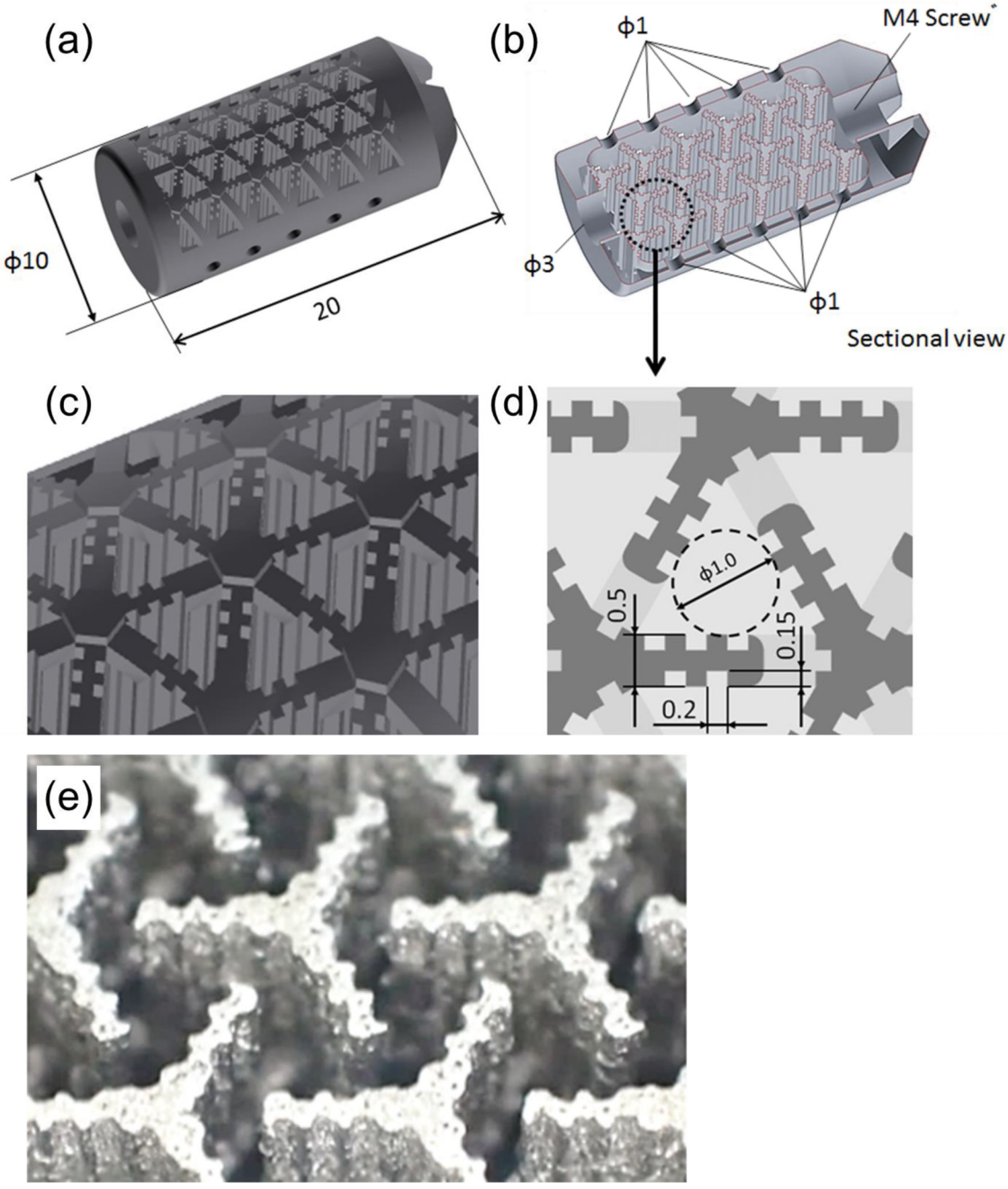

Fig. 2. Novel cage design with a through-pore with grooved substrate developed in this study. (A) Model of the entire cage and (B) half-section with indications of external dimensions. (C) Magnified image of the cage surface and (D) a schematic of through-pore with grooved substrate representing the design dimensions. (E) Picture of the through-pore with grooved substrate manufactured using laser powder bed fusion technology. Unit: mm.

Group_B_para: Type_B cage *without* an autologous bone graft, implanted such that the direction of the pores and grooves was *parallel* to the cephalocaudal axis.

Group_B_perp: Type_B cage *without* an autologous bone graft, implanted such that the direction of the pores and grooves was perpendicular to the cephalocaudal axis.

Group_C: Type_C cage with an autologous bone graft in the central hole, implanted such that the direction of the pores and grooves was *parallel* to the cephalocaudal axis.

To eliminate the effect of lumbar spine order, cages in the four groups were embedded in L1−L4 according to the following four patterns: (Group_A; Group_B_para; Group_B_perp; Group_C), (Group_B_para; Group_B_perp; Group_C; Group_A), (Group_B_perp; Group_C; Group_A; Group_B_para), and Group_C; Group_A; Group_B_para; Group_B_perp) for L1, L2, L3, and L4, respectively. As presented in Supplementary Fig. 4Sb, the autologous bone, which included cortical and trabecular

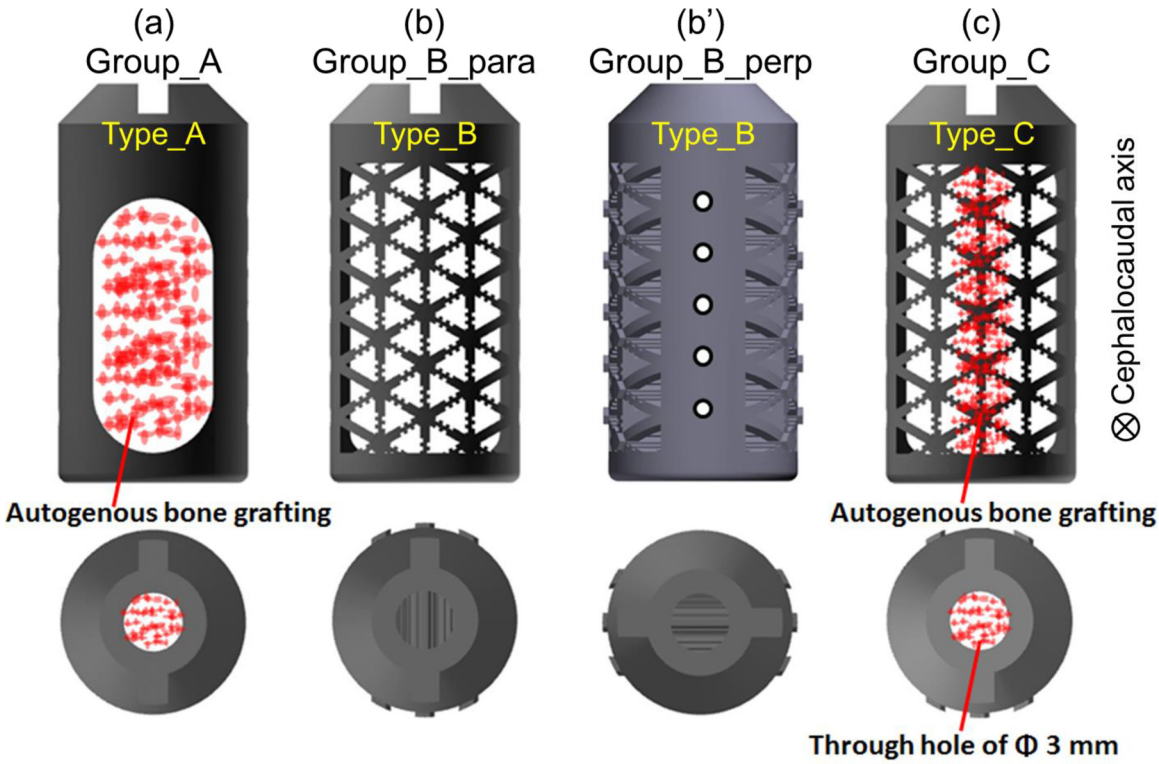

Fig. 3. Illustration of three types of spinal cages, indications of autologous bone use, and implantation direction with regard to the cephalocaudal axis. Four experimental groups were prepared. (A) Group_A: Type_A cage with an autologous bone graft in the central open pore was implanted such that the pore penetrated the cephalocaudal axis, (B) Group_B_para: Type_B cage with HTS without autologous bone graft was implanted such that the direction of the pores and grooves is parallel to the cephalocaudal axis, (B') Group_B_perp: Type_B cage with HTS without an autologous bone graft was implanted such that the direction of the pores and grooves is perpendicular to the cephalocaudal axis, and (C) Group_C: Type_C cage with HTS and autologous bone graft in the central hole was implanted such that the direction of the pores and grooves is parallel to the cephalocaudal axis.

bones, was obtained from the right iliac crest of the same animal using a rongeur. After removal of cartilage tissues, the iliac crest bone was crushed with an electric bone mill (Midas Rex BM120; Medtronic, MN, USA) into bone fragments of approximately 1 mm [30]. Photographs of the cages (Type_A and Type_C) after filling with autologous bone are shown in Supplementary Fig. 4Sc. The masses of introduced autologous iliac bone for Group_A and Group_C were 0.64±0.04 g and 0.12±0.02 g, respectively (n=8). Pedicle screws and spinal rods were not installed. The incision was sutured and disinfected. Calcein green (Dojindo, Kumamoto, Japan) was intravenously injected (25 mg/kg) for bone labeling. Sheep were provided *ad libitum* access to food and tap water. Animals were euthanized using bolus intravenous injections of pentobarbital sodium at 8 or 16 weeks post-surgery (n=4), as previously described [31,32], and the L1−L4, including the cages, were removed. The bone specimens were kept frozen at -80 ˚C until the pull-out test was performed.

Micro-computed tomography (μCT)

μCT (SMX-100CT; Shimadzu, Kyoto, Japan) was performed at 70 kV and 70 μA to produce 3D images with a spatial resolution of 57 μm on each side. The installation position of each cage and bone ingrowth into the cage were examined. Due to artifacts from Ti-6Al-4V, it was not possible to quantitatively evaluate bone volume fraction inside the cage from μCT images. Histological images were used to measure bone volume fraction, as described later.

Mechanical evaluation with the pull-out test

A pull-out test (Instron-5965; Instron, Norwood, MA, USA) was performed to evaluate the mechanical integrity of the cage/bone interface. To apply the pull-out load parallel to the long axis of the cage, M4 screws were used to connect the cage and crosshead. Next, the bone was fixed to the bottom of the testing space by using a room temperature polymerization resin (Ostron II; GC, Tokyo, Japan). The pull-out test was performed at a crosshead speed of 5 mm/min according to the ASTM F543-17 standard [33] until the cage was completely removed from the vertebral body. The pulled-out cage with bone tissue inside was immersed in 70% ethanol. Using the same pull-out setup, the mechanical property (braking load) of the non-implanted cage also was measured.

Specimen preparation

After the pull-out test, cages and associated bone tissue were embedded in methyl methacrylate. Specimens of 500 μm and 100 μm thickness were sectioned along the

dorsal plane (Group_A, Group_B_para, and Group_C) or transverse plane (Group_B_perp) from the center of the cage. Note that in Group_B_perp, specimens were sectioned in a different anatomical plane to analyze bone ingrowth along the groove.

Analysis of apatite c-axis orientation

The quality of the bone inside and surrounding the cage was evaluated based on the preferential orientation of the apatite *c*-axis using 500-μm-thick specimens. A microbeam X-ray diffractometer with a transmission optical system (R-Axis BQ; Rigaku, Tokyo, Japan) was employed to analyze the preferential orientation of the apatite *c*-axis. Mo-Kα radiation was generated at 50 kV and 90 mA. The incident beam was collimated into a 200-μm circular spot using a double-pinhole metal collimator and projected vertically onto each specimen to analyze the 2-D distribution of the apatite *c*-axis orientation along the surface of the thin specimen. Diffracted X-rays were collected for 300 s using an imaging plate placed behind specimens.

Based on the Debye ring obtained, the diffraction intensities (I) of the (002) and (310) planes of the biological apatite were integrated along the azimuthal angle (β) at angle steps of 1°. The (002) crystal plane was considered the representative plane of the apatite *c*-axis, and the (310) plane was orthogonal to the (002) plane. The intensity distributions as a function of β ($I(\beta)$) were approximated with the following elliptic polynomial function (subtracted by a constant c) using the least squares method [34]:

$$I(\beta) = \left\{ \frac{\cos^2(\beta-\mu)}{\alpha^2} - \frac{\sin^2(\beta-\mu)}{b^2} \right\}^{\frac{1}{2}} - c$$

In this equation, a, b, c, and μ are the fitting parameters, and μ is the angle at which the intensity peaks. The degree of apatite *c*-axis alignment was calculated as the intensity ratio of (002)/(310) for each β, resulting in a 2-D apatite *c*-axis orientation along the plane vertical to the incident X-ray beam. The 2-D distribution of apatite orientation was expressed as a radar diagram, and the value in the cephalocaudal axis was used for analysis.

Histology and analysis of collagen orientation

Specimens of 100-μm thickness prepared after the pull-out test were used for undecalcified Villanueva bone staining. The bone volume fraction (BV/TV, %) was determined. Histological and polarized images were obtained using an optical microscope (BX60; Olympus, Tokyo, Japan). A 2D birefringence analyzer (WPA-micro, Photonic Lattice, Sendai, Japan) was employed to assess collagen orientation [10]. For birefringence analysis, three polarized monochromatic lights with wavelengths of 523, 543, and 575 nm, respectively, were used in conjunction with 5 × and 10 × objective lenses. Given that collagen is a positive birefringent material, the optical fast and slow axes lie orthogonal and parallel, respectively, to the long axis of the collagen fibers [35]. Therefore, we analyzed the slow-axis direction for preferential collagen orientation.

Statistical analyses

Quantitative results are expressed as the mean±standard deviation. To compare data between two groups (8 vs. 16 weeks), a two-tailed unpaired Student's t test was used. To compare data among the four experimental groups, a one-way analysis of variance and post-hoc Tukey HSD multiple comparison were performed. Statistical significance was set at $p<.05$. SPSS version 25 software (IBM, IL, USA) for Microsoft Windows was used for all statistical analyses.

Results

Cage soundness, placement, and bone formation around and inside the cage

The 3D-CT images of the vertebrae after insertion of cages are presented in Supplementary Fig. 5S. The μCT images of sheep vertebral bodies in the median, transverse, and dorsal planes, including the cage, at 16 weeks are presented in Fig. 4. The cages were placed in the vertebral bodies without brokage or rotation. Pore direction was parallel to the cephalocaudal axis in Group_A, Group_B_para, and Group_C, whereas it was perpendicular to the cephalocaudal axis in Group_B_perp. The grooves of the HTS were not clearly visible at this resolution. In the conventional cage with autologous bone graft (Group_A), abundant bone was observed throughout the inner space. However, the bone (trabecular) morphology in the pore was not aligned in the cephalocaudal axis, thus, the continuity of trabeculae inside and outside the cage was poor. In contrast, bone morphology outside the cage adopted a preferential trabecular alignment along the cephalocaudal axis. In Group_B_para, Group_B_perp, and Group_C, no signs of bone resorption around the cage were noted, indicating that the cage and bone were in direct contact. Bone ingrowth inside the cage could not be observed due to artifacts of Ti-6Al-4V.

Mechanical integrity of the bone/cage interface

The breaking force of the non-implanted cage was 4021± 6 N. Typical load-displacement curves and maximum load for each group evaluated using the pull-out test are presented in Fig. 5. The maximum load at 8 and 16 weeks post-implantation was significantly lower in Group_A than that in the groups with HTS. No significant differences were observed in maximum load among the three groups (Group_B_para, Group_B_perp, and Group_C) with grooved substrates. In Group_A and Group_C, which contained autologous bone grafts, the maximum load increased significantly from 8 to 16 weeks post-surgery. Images of the cages after the pull-out test are presented in Fig. 6. In Group_B_para, Group_B_perp, and Group_C, abundant bone tissue was observed

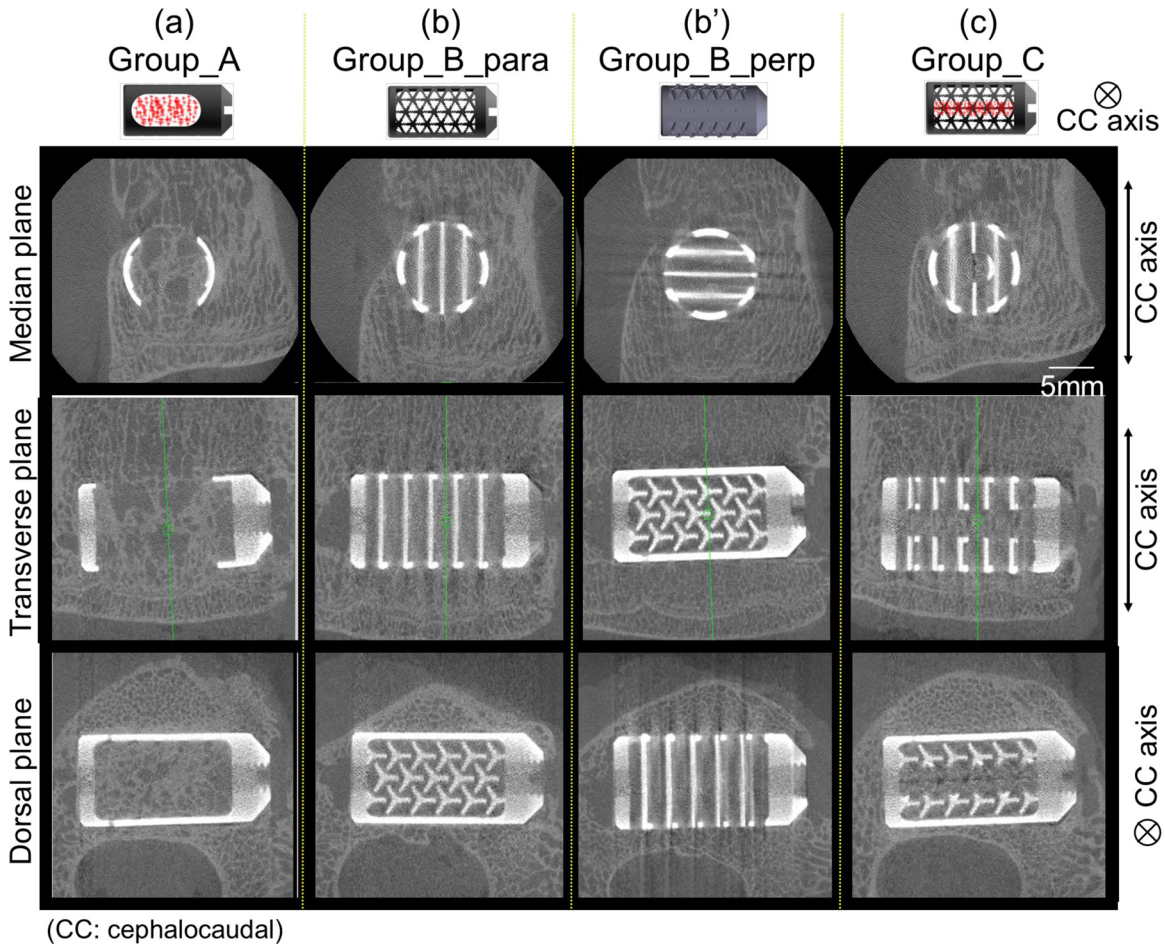

Fig. 4. Micro-computed tomography images of sheep vertebral bodies in the median, transverse, and dorsal planes including the central section of the cage at 16 weeks post-implantation. The cages were placed as planned without any obvious adverse events such as rotation, subsidence, or bone resorption around the cage.

around the cage openings even after the pull-out test. This suggested that new bone penetrated the HTS inside the cage, and bone tissues inside and outside the cage were interconnected and achieved functional fusion, resulting in superior mechanical strength.

Bone ingrowth into the cage

Typical Villanueva bone staining images at 8 and 16 weeks are depicted in Fig. 7. The bone volume fraction (BV/TV) values are summarized in Table. For Group_A and Group_C with autologous bone graft, the BV/TV was somewhat lower at 8 weeks and tended to increase by 16 weeks post-implantation (p=.055 and .075, respectively). Grafting autologous bone seems to have a tendency to delay bone formation.

At 8 weeks, the bones inside the cage of Group_A were gathered at the bottom of the cage following the pull-out test (Fig. 7A1), which reflects the very low interface bonding strength represented in Fig. 5. Note that this histology at 8 weeks does not reflect the situation when the cage was present in the vertebral body. In the groups (Group_B_para, Group_B_perp, and Group_C) with a grooved HTS substrate, the bone structure was preserved after the pull-out test, even outside the cage surface, suggesting that the cage and surrounding bone were tightly bound via newly formed bone and functioned integrally as a cage/bone system. In Group_B_para and Group_B_perp (at 8 weeks), trabeculae-like bone resembling normal trabecular bone penetrated from the ends of the cage (Supplementary Fig. 6S) and extended to the center (Fig. 7B1 and B'1). In Group_C, abundant bone was observed in the central pore at 8 weeks (Fig. 7C1); however, these bone fragments were not stained with calcein (Fig. 7D1 and E1), indicating that they were not newly formed but constituted autologous bone that had existed since the time of surgery. By 16 weeks postoperatively, remaining autologous bone fragments were replaced (Fig. 7D2 and E2). In Group_B_perp, the bone morphology inside the cage changed significantly from trabecular-like to a rounded shape at 16 weeks, and bone connectivity was lost (Fig. 7B'2).

Preferential orientation of apatite c-axis and collagen as a bone quality

The distribution of the degree of apatite *c*-axis orientation inside and outside the cage along the cephalocaudal

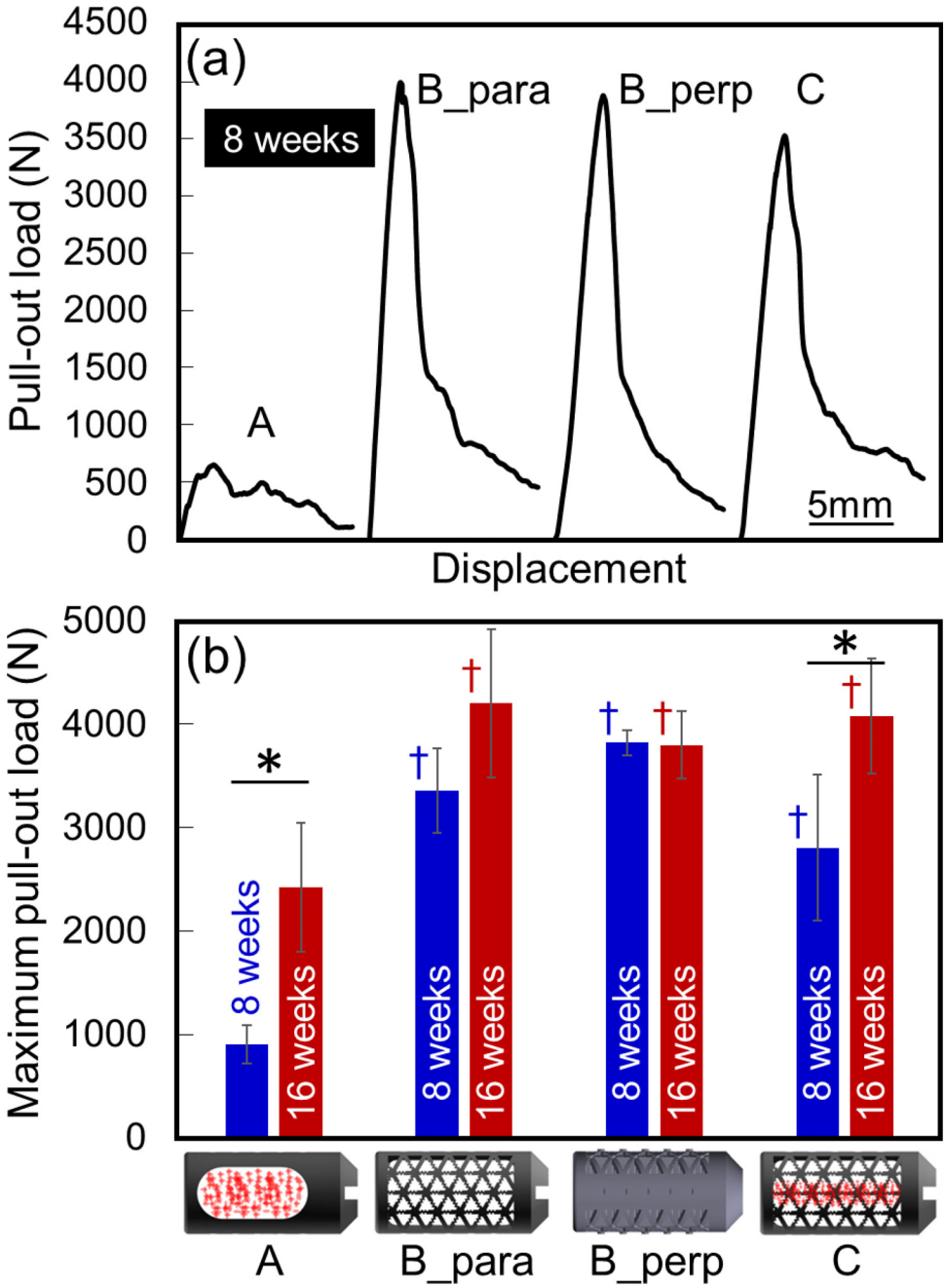

Fig. 5. Mechanical stability of the cage/bone interface evaluated using a pull-out test. (A) Typical pull-out load-displacement curves obtained at 8 weeks post-implantation and (B) variation in pull-out maximum load among groups and implantation periods. *p<.05 between groups (*t* test). †p<.05 versus Group_A (Tukey HSD multiple comparison test).

axis is presented in Fig. 8. Statistical differences among groups at the typical positions are presented in Fig. 8B-E and G-J. In Group_A, apatite orientation inside the cage remained low throughout the experimental period. Group_B_para exhibited a trend towards higher apatite orientation compared to normal trabeculae (p=.081), and this orientation was maintained until 16 weeks. Group_B_perp exhibited a higher orientation at 8 weeks, and the orientation exhibited a trend to be lower at 16 weeks (p=.065). At 8 weeks, orientation near the cage center was lower in Group_C than in Group_B (p<.05) (Fig. 8E) and was significantly increased at 16 weeks (p<.05). In Group_B_perp, orientation outside the cage was significantly lower due to the difference in the anatomical plane from which the section was prepared.

Data on the presence of HTS, groove direction, and presence of autologous bone are summarized as follows: (1) if HTS was parallel to the cephalocaudal axis (Group_B_para and Group_C), bone with highly oriented apatite *c*-axis along the cephalocaudal axis (groove direction) was

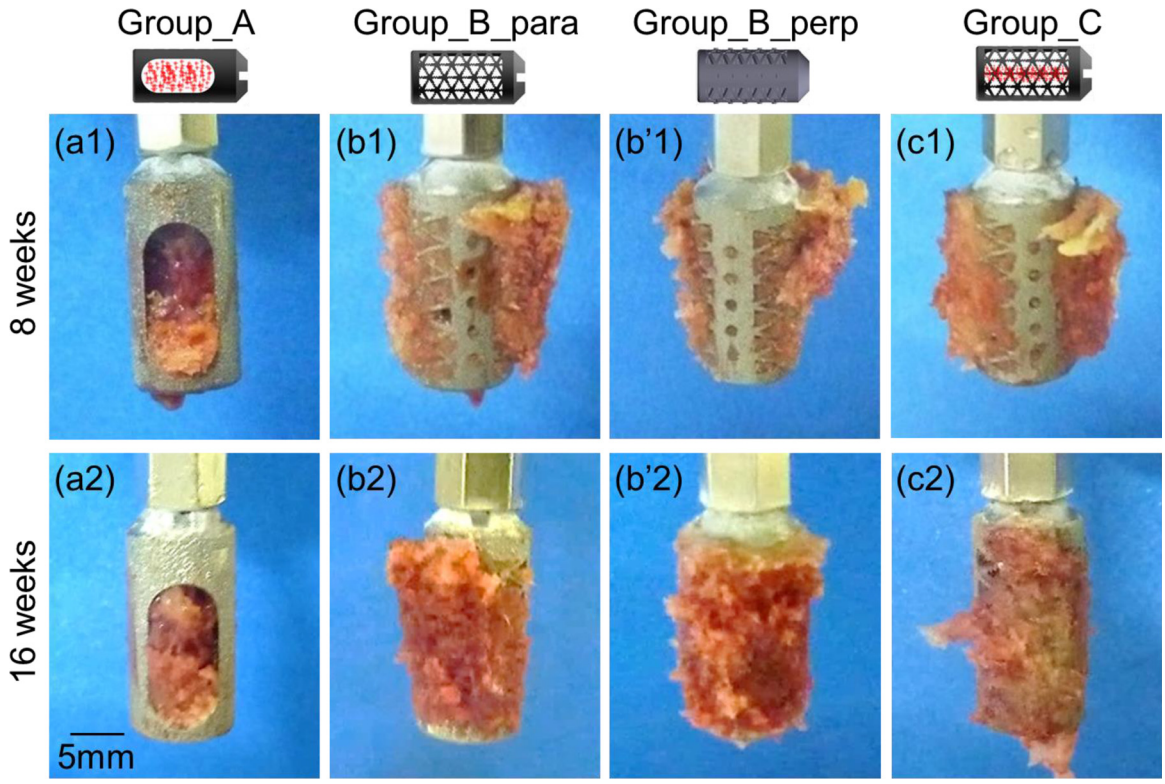

Fig. 6. Pictures of the cages after the pull-out test at 8 and 16 weeks post-implantation. In Group_B_para, Group_B_perp, and Group_C, abundant bone tissue remained around the cage openings, indicating adequate interfacial bonding strength between the cage and host bone. The cage was mechanically and functionally fused with host bone, which enabled cage stabilization.

induced; (2) autologous bone delayed the increase in apatite orientation (Group_C); (3) if HTS was perpendicular to the cephalocaudal axis (Group_B_perp), bone with relatively high apatite orientation along the groove direction was formed during the initial stage, but the degree of orientation decreased after a long period of implantation; and (4) in the absence of HTS, bone without a specific orientation was formed.

Collagen orientation maps around the bone-cage interface for Group_B_para and Group_B_perp are depicted in Fig. 9. Inside the cage, collagen was aligned parallel to the groove direction in both groups, which corresponded well with the apatite *c*-axis orientation. In Group_B_perp, collagen orientation direction was drastically altered between the inside and outside of the cage, indicating that the grooved substrate of HTS strongly induced bone with collagen orientation in a completely different direction to that of the original orientation.

Factors determining bone/cage interfacial strength

The associations between pull-out load and BV/TV, and pull-out load and degree of apatite orientation are presented in Supplementary Fig. 7S. Pull-out load correlated weakly with BV/TV at 8 weeks and strongly with apatite orientation at 8 and 16 weeks post-surgery. Thus, the bone/cage interfacial strength was governed by apatite orientation rather than BV/TV, justifying our design strategy and decision to induce bone with a highly oriented ECM.

Discussion

The present study investigated the potential of a novel spinal cage with HTS developed using a design strategy for inducing an anisotropic trabecular microstructure. Our novel cage enabled functional bonding to the surrounding trabecular bone by inducing new trabecular-like bone with a highly oriented collagen/apatite micro-organization along the cephalocaudal axis, in which principal stress is applied.

Validation of the sheep model to ensure clinical relevance

Although the sheep model is frequently used in the study of spinal devices [36,37], the use of sheep to assess the therapeutic value of spinal devices should first be discussed from a biomechanical perspective. The largest difference between bipeds and sheep, which are quadrupeds, is the direction of the spine axis, which is vertical in humans and horizontal in sheep. Nevertheless, the sheep spine has been reported to exhibit similarities to the human spine in its geometry [25], mechanical properties [26], and anisotropy of lumbar trabecular bone [24]. Wang et al. [24] reported that the trabeculae preferentially run parallel to the cephalocaudal axis in the lumbar vertebrae of both humans and

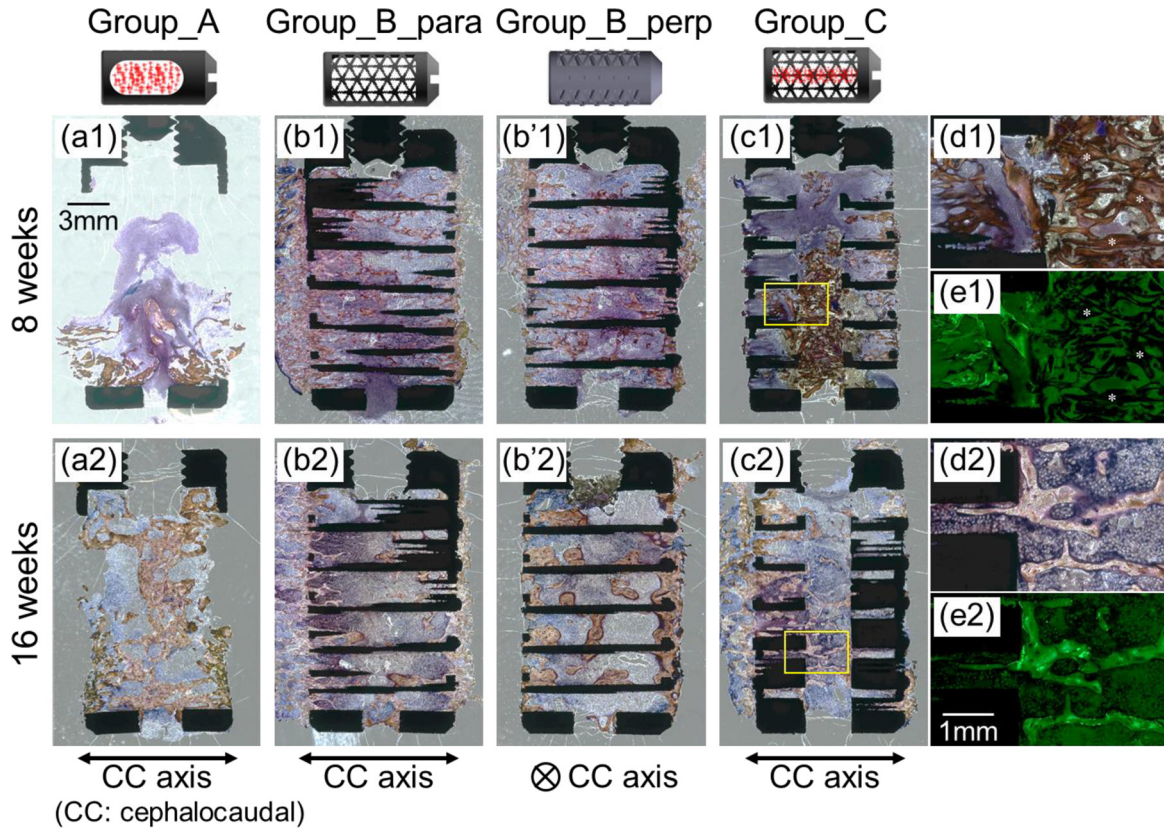

Fig. 7. Histological evaluation of the cage. Typical Villanueva bone staining images at (A1-C1) 8 and (A2-C2) 16 weeks post-implantation. Magnified images and corresponding calcein fluorescence images of the boxed regions at (D1, E1) 8 and (D2, E2) 16 weeks post-implantation. * indicates remaining autologous bone without signs of calcein incorporation.

sheep, which substantiates the fact that the vertebral body in both sheep and humans is predominantly loaded along the cephalocaudal axis, in accordance with Wolff's law. Although a higher axial stress is expected in sheep vertebrae due to higher trabecular density [38] and more trabeculae running along the cephalocaudal axis [24], biped and quadruped spines are substantially loaded in a similar way. Hence, research using sheep models is useful for developing spinal devices for use in humans. From this perspective, the results of this study, as well as the following discussion, have clinical relevance.

Effects of HTS and cage implantation direction

The conventional cage (Group_A) without HTS formed new bone that lacked the anisotropic features of spinal trabecular bone, leading to poor continuity of trabeculae inside and outside the cage (Fig. 4A). In contrast, the HTS implant parallel to the anisotropy of normal trabecular bone (Group_B_para) led to the development of new bone with trabecular-like morphology along the through-pores. Good continuity of trabecular architecture inside and outside the cage was achieved, indicated by trabeculae that were connected in an almost one-to-one correspondence at the cage/bone interface (Fig. 7B1 and B2). The design concept of the HTS pore diameter for reproducing the original trabecular structure must have been beneficial. In addition, the newly formed trabecular-like bone inside the cage showed preferentially oriented ECM which was similar to the intact trabeculae along the through-pores and grooves. The ECM orientation in the new bone inside the cage tended to be higher than that in the normal trabecular bone (blue dashed

Table
Bone volume fraction (BV/TV) inside the cage for each group at 8 and 16 weeks post-implantation

	Group_A	Group_B_para	Group_B_perp	Group_C
8 weeks	12.0±6.8	16.7±8.7	22.1±6.1	12.3±7.9
16 weeks	25.5±9.1	13.3±7.0	26.5±11.7	24.5±8.2

No significant differences were observed, but for Group_A and Group_C, the BV/TV at 8 weeks tended to be lower than that at 16 weeks post-implantation (p=.055 and .075, respectively) (*t* test).

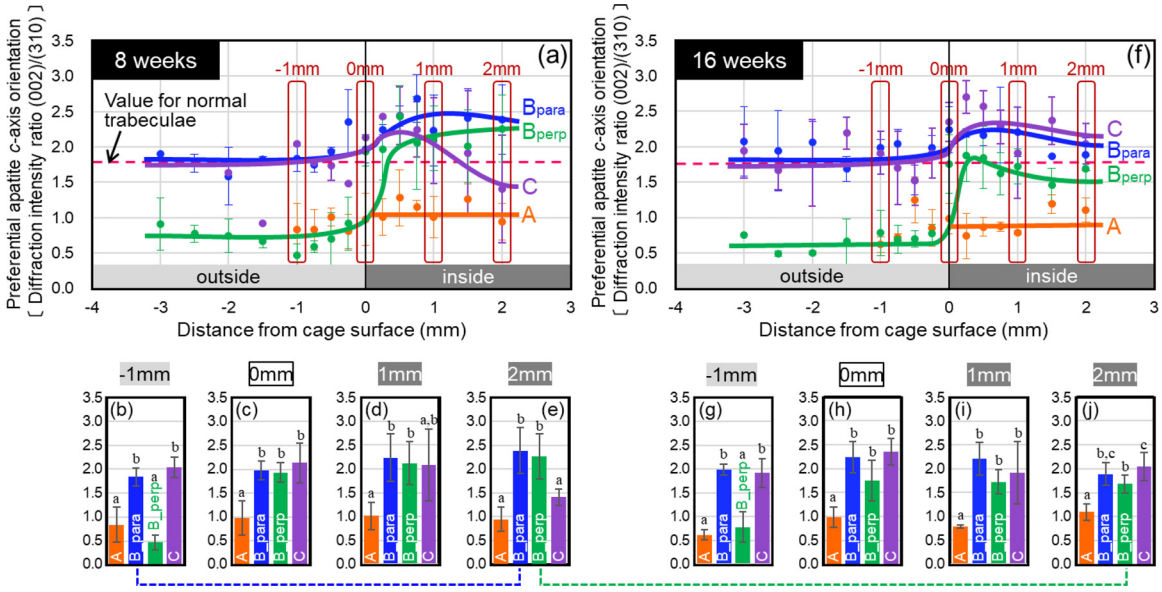

Fig. 8. Distribution of the degree of preferential apatite *c*-axis orientation along the cephalocaudal axis inside and outside of the cage at (A) 8 and (F) 16 weeks post-implantation. (B-E, G-J) The data at -1, 0 (interface), 1, and 2 mm are extracted to indicate statistical differences. a, b, and c indicate homogeneous subgroups with p<.05 (Tukey HSD multiple comparison test). Blue and green dashed lines at the bottom indicate a trend for a significant difference (p<.1) (*t* test).

line at the bottom of Fig. 8). Notably, even when the HTS was embedded in the direction perpendicular to the anisotropy of normal trabecular bone (Group_B_perp), we observed new bone with an ECM orientation in the direction of the through-pore and grooved substrate, which was distinct from the original orientation direction. In the initial stage of bone regeneration, immature bone with randomly oriented ECM is formed, and the recovery of ECM orientation takes 24 weeks [6]. The full recovery of ECM orientation is a lengthy process as it requires replacement (remodeling) of the initially formed immature bone. However, HTS directly induced bone with a highly oriented ECM comparable to that of normal trabeculae, which was demonstrated *in vitro*. The grooved substrate may have provided a cue to induce bone microstructural anisotropy even *in vivo*.

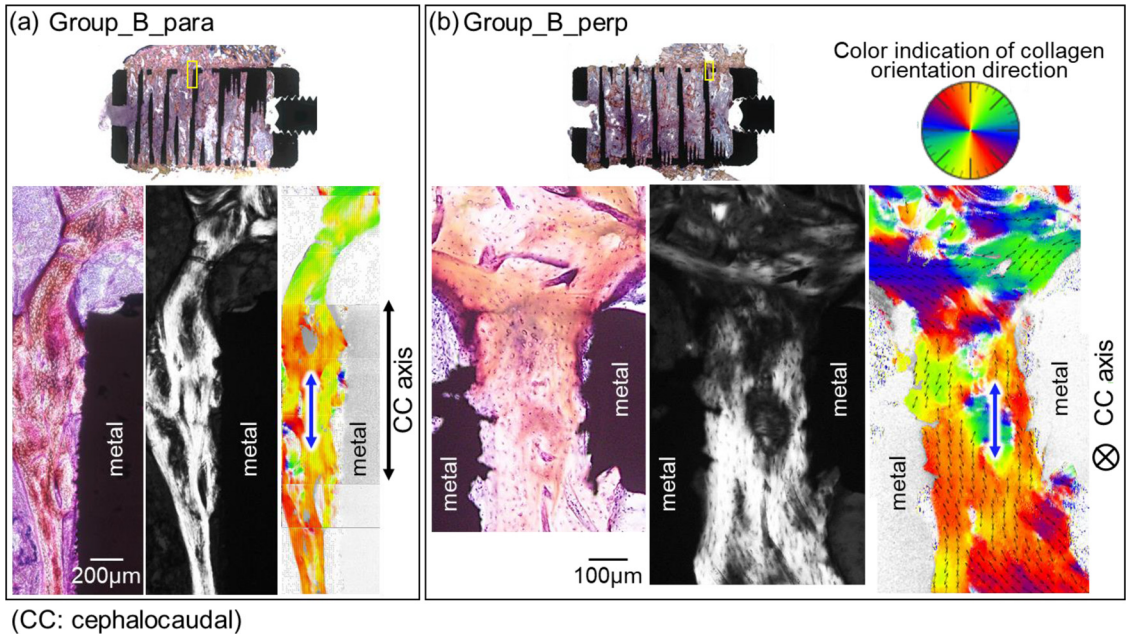

Fig. 9. Collagen orientation distribution around the bone-cage interface for (A) Group_B_para and (B) Group_B_perp. Optical images, polarized images, and color maps obtained using birefringence microscopy indicating collagen orientation direction obtained for the boxed regions. Bright contrast in the polarized image represents collagen orientation along the vertical direction of the paper surface (parallel to the through-pore and elongated groove direction).

When HTS was implanted in a direction orthogonal to normal trabecular bone anisotropy (Group_B_perp), oriented ECM was initially formed, but the orientation tended to decrease after 16 weeks (green dashed line at the bottom of Fig. 8). Furthermore, the bone adopted a rounded, isotropic morphology. As the through-pore direction was perpendicular to the cephalocaudal axis (principal stress direction), the bone inside the cage may not have been loaded by stress along the pore direction. Indeed, it is well-established that trabecular morphology is formed along stress flow lines [39,40]. As such, even if anisotropic bone with oriented ECM is formed at the initial stage, the anisotropy cannot be maintained unless a robust stress is applied. This is also supported by the significant deterioration in ECM orientation along the long axis of long bones following stress removal by neurectomy [41].

In Group_B_para, osteocytes elongated in the through-pore direction of the HTS (Supplementary Fig. 8S). Osteocytes are thought to play pivotal roles in the maintenance of bone mechanical integrity via mechanosensing capabilities [42,43]. Nevertheless, the factors regulating the alignment of osteocytes are unclear; one possibility is that osteocytes inherit the alignment of osteoblasts on the groove surface. The periodic groove structure designed in this study activated the unidirectional arrangement of cultured osteoblasts along the groove direction. In Group_B_para, the through-pore direction of HTS coincided with the cephalocaudal axis (ie, principal stress direction). The alignment of osteocyte cell bodies parallel to the principal stress direction suggests increased stress sensitivity based on the fluid flow theory in canaliculi, which extends preferentially in the direction perpendicular to the elongated direction of the cell body [44].

These results indicate that HTS with grooved substrate has the ability to induce bone with sound ECM orientation and may align osteocytes for mechanosensing from the initial stage. Further, the through-pore may facilitate stress flow through new bone in the pore. By orienting the direction of the groove and through-pore parallel to the principal stress direction (cephalocaudal axis in this case), it is possible to induce bone with structural anisotropy at two scales, namely trabecular macroscopic architecture and nano-arrangement of ECM in the trabeculae.

Potential of novel cage structure to replace autologous bone grafts

The use of a box-type cage with autologous iliac crest bone grafting has long been the gold standard. Autologous bone grafts are used for osteogenic, osteoinductive, and osteoconductive capacity, and are predominantly derived from bone marrow containing a large number of surviving bone marrow cells [45]. Direct evidence for the advantageous effects of autologous bone grafts on cage fusion is scarce. There is limited literature reporting that autologous iliac bone grafts slightly increase bone formation in box-type cages [46]. The novel cage developed in this study (Group_B_para and Group_C) exhibited significantly higher pull-out strength compared to the conventional box-type cage with an autologous bone graft (Group_A), even without an autologous bone graft (Group_B_para) (Fig. 5). No significant difference in strength was observed between Group_B_para and Group_C; however, the increase in strength in Group_C tended to lag (Fig. 5), clearly indicating that the beneficial effects of the novel cage structure with HTS (through-pore with grooved substrate) far exceeded that of autologous bone grafts. A similar decreasing trend in apatite orientation was observed in Group_C. Apatite orientation near the cage center in Group_C at 8 weeks was relatively low while increasing by postoperative week 16. As autologous bone requires resorption prior to new bone formation, bone formation and maturation are delayed. Autologous bone remained inside the cage after 8 weeks (Fig. 7E1). The relationship between the presence of autologous bone, the delayed bone formation, and their effects on the decreased ECM orientation needs to be investigated at the molecular level. Here, it should be noted that the bone marrow from the autologous bone contains factors contributing to osteogenic events as well as factors contributing to bone resorption, such as osteoclasts.

In contrast, HTS provided a scaffold for bone formation even deep within the cage, enabling direct bone formation without the need for autologous bone resorption. Thus, this novel structure may replace or even provide a superior alternative to autologous bone grafts inside the cage. This is due to the ability of HTS to continuously induce preferentially oriented ECM and formation of strengthened bone along the principal stress direction (cephalocaudal axis) at the cage-host bone interface (blue lines in Fig. 8A and B). Moreover, the through-pore with grooved substrate itself exhibits an anisotropic architecture resembling that of original trabecular bone. By serially connecting with the new bone inside the cage, it may even contribute to mutual stress transmission with bone.

Various grafting options have recently been developed, including allograft-based, synthetic, growth factor- and cell-based materials, genetic therapy, and combined approaches [47]. Each of these options has advantages and disadvantages, and the optimal application in clinical settings remains controversial. Thus, the cage proposed in this study represents an innovative high-performance spinal cage that does not require autologous bone and/or artificial graft materials inside the cage.

Limitations

Cages are typically inserted in the intervertebral space to achieve fusion of destabilized vertebral bodies and mechanically stabilize them. A major limitation in this study is the cage embedment within the vertebral body. The main purpose of this study was to investigate the osteoconductive capacity of a newly designed cage for guiding bones with

anisotropic macro-architecture and ECM nano-arrangement. Given that the cage was completely surrounded by trabecular bone, it was possible to clarify the intrinsic potential of the cage's osteoconductivity and the effects of implantation direction. Our next challenge is to deploy this advantageous design in an intervertebral fusion cage. To achieve this, it is necessary to discuss the difference in conditions to which the cage is exposed. The major difference that should be taken into account between inside the vertebral body and intervertebral space would be the mechanical environment. In the case that the cage is embedded inside the vertebral body, the cage would be shielded from the *in vivo* loads that the cage is subjected to, compared to the case that the cage is implanted in the intervertebral space. To accommodate this, it is necessary to update the shape and thickness of the outer shell and the thickness of the HTS to ensure the strength of the cage even when the cage is implanted in the intervertebral space. The mechanical integrity of the cage should be thoroughly verified for use in the intervertebral space, which is important due to the unique mechanical properties of PBF-LB-printed material [48]. In addition, it is assumed that cells are relatively less likely to be recruited and thus osteoconductivity is inferior in the intervertebral space than in the vertebral body, which is filled with bone marrow. The introduction of autologous bone marrow or external factors such as cytokines into the cage might be necessary to promote osteoblast recruitment and ensure sufficient osteoconductivity in the intervertebral space.

Moreover, we did not obtain collateral data that adequately explain the variation in BV/TV and ECM orientation over time or between groups. Further investigation including biological evaluation is needed to elucidate the factors contributing to the high osteoconductivity of the newly developed cages.

Future perspectives

Additive manufacturing is convenient for altering the shape parameters and introducing size variations; its usefulness as a means of fabricating spinal devices has been recognized [37,49]. Moreover, approximating the mechanical properties of the cage material to that of trabecular bone will be critical for suppressing bone fracture at the devise/bone interface (cage subsidence) and stress-shielding [50]. By employing a β-titanium alloy (for example, ISO-approved Ti-15Mo-5Zr-3Al) with a low Young's modulus as a material and developing the crystallographic texture using additive manufacturing [51], it is possible to further reduce the Young's modulus [52]. Additive manufacturing will enable the development of a spinal device with high performance in terms of both shape for inducing anisotropic bone and material properties with low Young's modulus.

Conclusions

In the present study, we introduced a novel design concept for spinal cages that induces a sound trabecular bone-mimetic new bone characterized by anisotropic trabecular architecture strengthened by preferentially oriented ECM along the cephalocaudal axis which corresponds to the principal stress direction. A cage with HTS composed of through-pore and grooved substrate was designed and manufactured using 3D printing technology (PBF-LB) and subsequently implanted in the sheep vertebral body. Our major findings are summarized below:

The newly designed cage with HTS induced hierarchically anisotropic trabecular-like bone with preferentially elongated trabeculae at micro-millimeter scale and ECM orientation at nanometer scale within a trabecula, both of which were parallel to the through-pore and groove direction. This hierarchical anisotropic structure, mimetic to normal trabecular bone, was already formed 8 weeks following cage implantation, which was independent on the implantation direction. HTS was shown to have a strong ability to guide ECM-oriented functional bone.

The novel cage exhibited substantially greater strength at the cage/host bone interface at 8 weeks post-implantation than a conventional and gold-standard box-type cage with autologous iliac bone graft, even without the introduction of autologous bone inside the cage. We showed that the HTS equipped in the new cage aids the rapid recovery of mechanical functions.

HTS eliminates the need for a secondary surgery for autologous bone harvesting and contributes to the reduction of invasiveness and various burdens associated with the additional operation.

Furthermore, autologous bone tended to delay bone formation in the cage and maturation due to the need for absorption. It was suggested that the introduction of autologous bone may have a negative effect on the functional recovery of the bone, which needs to be further verified.

HTS provided a direct scaffold for bone formation with ECM orientation (even in the case that the HTS was implanted perpendicular to the cephalocaudal axis), resulting in functional fusion between the cage and bone at an early stage. This novel concept provides useful guidelines for the design of highly functionalized spinal devices in the future.

Declarations of competing interests

Manabu Ito is the chairperson of the AOSpine Asia Pacific. The other authors declare that they have no conflict of interest.

Acknowledgments

This study was supported by Grants-in-Aid for Scientific Research (JP18H05254) from the Japan Society for the Promotion of Science (JSPS) and the Strategic Promotion of Innovative Research and Development (S-Innovation) from the Japan Agency for Medical Research and Development (AMED). The authors gratefully acknowledge technical

support in animal experiment by Hidekazu Yoshizaki at Hokkaido Medical Center.

Authors' roles

Takuya Ishimoto: Acquisition and data, Analysis and interpretation of data, Drafting of the manuscript, Statistical analysis; **Yoshiya Kobayashi**: Acquisition and data, Analysis and interpretation of data; **Masahiko Takahata**: Analysis and interpretation of data, Critical revision of the manuscript for important intellectual content; **Manabu Ito**: Conception and design (animal study), Analysis and interpretation of data, Critical revision of the manuscript for important intellectual content; **Aira Matsugaki**: Acquisition and data, Analysis and interpretation of data, Critical revision of the manuscript for important intellectual content; **Hiroyuki Takahashi**: Acquisition and data, Analysis and interpretation of data, Critical revision of the manuscript for important intellectual content; **Ryota Watanabe**: Acquisition and data, Analysis and interpretation of data; **Takayuki Inoue**: Acquisition and data, Analysis and interpretation of data; **Tadaaki Matsuzaka**: Acquisition and data, Analysis and interpretation of data; **Ryosuke Ozasa**: Acquisition and data, Analysis and interpretation of data; **Takao Hanawa**: Supervision; **Katsuhiko Yokota**: Supervision; **Yoshio Nakashima**: Supervision; **Takayoshi Nakano**: Conception and design (all study containing the cage design), Analysis and interpretation of data, Obtaining funding, Supervision.

Supplementary materials

Supplementary material associated with this article can be found in the online version at https://doi.org/10.1016/j.spinee.2022.05.006.

References

[1] Singh G, Hsu WK. Fusion biologics and adjuvants in minimally invasive spine surgery. Minimally Invasive Spine Surgery. New York: Springer International Publishing; 2020. p. 101–16. https://doi.org/10.1007/978-3-030-19007-1_10.

[2] Egol KA, Nauth A, Lee M, Pape HC, Watson JT, Borrelli Jr. J. Bone grafting: sourcing, timing, strategies, and alternatives. J Orthop Trauma 2015;29:S10–4. https://doi.org/10.1097/BOT.0000000000000460.

[3] Landis WJ. The strength of a calcified tissue depends in part on the molecular structure and organization of its constituent mineral crystals in their organic matrix. Bone 1995;16:533–44. https://doi.org/10.1016/8756-3282(95)00076-P.

[4] Ozasa R, Ishimoto T, Miyabe S, Hashimoto J, Hirao M, Yoshikawa H, et al. Osteoporosis changes collagen/apatite orientation and Young's modulus in vertebral cortical bone of rat. Calcif Tissue Int 2019;104:449–60. https://doi.org/10.1007/s00223-018-0508-z.

[5] Ozasa R, Saito M, Ishimoto T, Matsugaki A, Matsumoto Y, Nakano T. Combination treatment with ibandronate and eldecalcitol prevents osteoporotic bone loss and deterioration of bone quality characterized by nano-arrangement of the collagen/apatite in an ovariectomized aged rat model. Bone 2022;157:116309. https://doi.org/10.1016/j.bone.2021.116309.

[6] Ishimoto T, Nakano T, Umakoshi Y, Yamamoto M, Tabata Y. Degree of biological apatite c-axis orientation rather than bone mineral density controls mechanical function in bone regenerated using recombinant bone morphogenetic protein-2. J Bone Miner Res 2013;28:1170–9. https://doi.org/10.1002/jbmr.1825.

[7] Tanaka Y, Kubota A, Matsusaki M, Duncan TJ, Hatakeyama Y, Fukuyama K, et al. Anisotropic mechanical properties of collagen hydrogels induced by uniaxial-flow for ocular applications. J Biomater Sci Polym Ed 2011;22:1427–42. https://doi.org/10.1163/092050610X510542.

[8] Viswanath B, Raghavan R, Ramamurty U, Ravishankar N. Mechanical properties and anisotropy in hydroxyapatite single crystals. Scr Mater 2007;57:361–4. https://doi.org/10.1016/j.scriptamat.2007.04.027.

[9] Nakano T, Kaibara K, Tabata Y, Nagata N, Enomoto S, Marukawa E, et al. Unique alignment and texture of biological apatite crystallites in typical calcified tissues analyzed by microbeam X-ray diffractometer system. Bone 2002;31:479–87. https://doi.org/10.1016/S8756-3282(02)00850-5.

[10] Ishimoto T, Yamada K, Takahashi H, Takahata M, Ito M, Hanawa T, et al. Trabecular health of vertebrae based on anisotropy in trabecular architecture and collagen/apatite micro-arrangement after implantation of intervertebral fusion cages in the sheep spine. Bone 2018;108:25–33. https://doi.org/10.1016/j.bone.2017.12.012.

[11] Miyabe S, Nakano T, Ishimoto T, Takano N, Adachi T, Iwaki H, et al. Two-dimensional quantitative analysis of preferential alignment of BAp c-axis for isolated human trabecular bone using microbeam X-ray diffractometer with a transmission optical system. Mater Trans 2007;48:343–7. https://doi.org/10.2320/matertrans.48.343.

[12] Manjubala I, Liu Y, Epari DR, Roschger P, Schell H, Fratzl P, et al. Spatial and temporal variations of mechanical properties and mineral content of the external callus during bone healing. Bone 2009;45:185–92. https://doi.org/10.1016/j.bone.2009.04.249.

[13] Chakkalakal DA, Strates BS, Mashoof AA, Garvin KL, Novak JR, Fritz ED, et al. Repair of segmental bone defects in the rat: an experimental model of human fracture healing. Bone 1999;25:321–32. https://doi.org/10.1016/S8756-3282(99)00167-2.

[14] Watanabe Y, Takai S, Arai Y, Yoshino N, Hirasawa Y. Prediction of mechanical properties of healing fractures using acoustic emission. J Orthop Res 2001;19:548–53. https://doi.org/10.1016/S0736-0266(00)00042-5.

[15] Kashii M, Hashimoto J, Nakano T, Umakoshi Y, Yoshikawa H. Alendronate treatment promotes bone formation with a less anisotropic microstructure during intramembranous ossification in rats. J Bone Miner Metab 2008;26:24–33. https://doi.org/10.1007/s00774-007-0782-8.

[16] Kerschnitzki M, Wagermaier W, Roschger P, Seto J, Shahar R, Duda GN, et al. The organization of the osteocyte network mirrors the extracellular matrix orientation in bone. J Struct Biol 2011;173:303–11. https://doi.org/10.1016/j.jsb.2010.11.014.

[17] Gui N, Xu W, Myers DE, Shukla R, Tang HP, Qian M. The effect of ordered and partially ordered surface topography on bone cell responses: a review. Biomater Sci 2018;6:250–64. https://doi.org/10.1039/C7BM01016H.

[18] Matsugaki A, Aramoto G, Nakano T. The alignment of MC3T3-E1 osteoblasts on steps of slip traces introduced by dislocation motion. Biomaterials 2012;33:7327–35. https://doi.org/10.1016/j.biomaterials.2012.06.022.

[19] Tamiello C, Buskermolen ABC, Baaijens FPT, Broers JLV, Bouten CVC. Heading in the right direction: understanding cellular orientation responses to complex biophysical environments. Cell Molecul Bioeng 2016;9:12–37. https://doi.org/10.1007/s12195-015-0422-7.

[20] Ozasa R, Matsugaki A, Isobe Y, Saku T, Yun HS, Nakano T. Construction of human induced pluripotent stem cell-derived oriented bone matrix microstructure by using in vitro engineered anisotropic

culture model. J Biomed Mater Res A 2017;106:360–9. https://doi.org/10.1002/jbm.a.36238.
[21] Wang JHC, Jia F, Gilbert TW, Woo SLY. Cell orientation determines the alignment of cell-produced collagenous matrix. J Biomech 2003;36:97–102. https://doi.org/10.1016/S0021-9290(02)00233-6.
[22] Matsugaki A, Isobe Y, Saku T, Nakano T. Quantitative regulation of bone-mimetic, oriented collagen/apatite matrix structure depends on the degree of osteoblast alignment on oriented collagen substrates. J Biomed Mater Res A 2015;103:489–99. https://doi.org/10.1002/jbm.a.35189.
[23] Biggs MLP, Richards RG, McFarlane S, Wilkinson CDW, Oreffo ROC, Dalby ML. Adhesion formation of primary human osteoblasts and the functional response of mesenchymal stem cells to 330-nm deep microgrooves. J R Soc Interface 2008;5:1231–42. https://doi.org/10.1098/rsif.2008.0035.
[24] Wang Y, Liu G, Li T, Xiao Y, Han Q, Xu R, et al. Morphometric comparison of the lumbar cancellous bone of sheep, deer, and humans. Comp Med 2010;60:374–9.
[25] Wilke HJ, Kettler A, Wenger KH, Claes LE. Anatomy of the sheep spine and its comparison to the human spine. Anat Rec 1997;247:542–55. https://doi.org/10.1002/(SICI)1097-0185(199704)247:4<542::AID-AR13>3.0.CO;2-P.
[26] Wilke HJ, Kettler A, Claes LE, Lutz E. Are sheep spines a valid biomechanical model for human spines? Spine 1997;22:2365–74. https://doi.org/10.1097/00007632-199710150-00009.
[27] Kennedy OD, Brennan O, Rackard SM, O'Brien FJ, Taylor D, Lee TC. Variation of trabecular microarchitectural parameters in cranial, caudal and mid-vertebral regions of the ovine L3 vertebra. J Anat 2009;214:729–35. https://doi.org/10.1111/j.1469-7580.2009.01054.x.
[28] Zarrinkalam MR, Beard H, Schultz CG, Moore RJ. Validation of the sheep as a large animal model for the study of vertebral osteoporosis. Eur Spine J 2009;18:244–53. https://doi.org/10.1007/s00586-008-0813-8.
[29] Müller R, Henss A, Kampschulte M, Rohnke M, Langheinrich AC, Heiss C, et al. Analysis of microscopic bone properties in an osteoporotic sheep model: a combined biomechanics, FE and ToF-SIMS study. J R Soc Interface 2019;16:20180793. https://doi.org/10.1098/rsif.2018.0793.
[30] Pelletier MH, Cordaro Punjabi VM, Waites M, Lau A, Walsh WR. PEEK versus Ti interbody fusion devices, resultant fusion, bone apposition, initial and 26-week biomechanics. Clin Spine Surg 2016;29:208–14. https://doi.org/10.1097/BSD.0b013e31826851a4.
[31] McGilvray KC, Easley J, Seim HB, Regan D, Berven SH, Hsu WK, et al. Bony ingrowth potential of 3D-printed porous titanium alloy: a direct comparison of interbody cage materials in an in vivo ovine lumbar fusion model. Spine J 2018;18:1250–60. https://doi.org/10.1016/j.spinee.2018.02.018.
[32] Yamada K, Ito M, Akazawa T, Murata M, Yamamoto T, Iwasaki N. A preclinical large animal study on a novel intervertebral fusion cage covered with high porosity titanium sheets with a triple pore structure used for spinal fusion. Eur Spine J 2015;24:2530–7. https://doi.org/10.1007/s00586-015-4047-2.
[33] ASTM F543-17. Standard Specification and Test Methods for Metallic Medical Bone Screws. West Conshohocken, PA: ASTM International; 2017.
[34] Noyama Y, Nakano T, Ishimoto T, Sakai T, Yoshikawa H. Design and optimization of the oriented groove on the hip implant surface to promote bone microstructure integrity. Bone 2013;52:659–67. https://doi.org/10.1016/j.bone.2012.11.005.
[35] Sekita A, Matsugaki A, Ishimoto T, Nakano T. Synchronous disruption of anisotropic arrangement of the osteocyte network and collagen/apatite in melanoma bone metastasis. J Struct Biol 2017;197:260–70. https://doi.org/10.1016/j.jsb.2016.12.003.
[36] Loenen ACY, Peters MJM, Bevers RTJ, Schaffrath C, van Haver E, Cuijpers VMJI, et al. Early bone ingrowth and segmental stability of a trussed titanium cage versus a polyether ether ketone cage in an ovine lumbar interbody fusion model. Spine J 2022;22:174–82. https://doi.org/10.1016/j.spinee.2021.07.011.
[37] Van Horn MR, Beard R, Wang W, Cunningham BW, Mullinix KP, Allall M, et al. Comparison of 3D-printed titanium-alloy, standard titanium-alloy, and PEEK interbody spacers in an ovine model. Spine J 2021;21:2097–103. https://doi.org/10.1016/j.spinee.2021.05.018.
[38] Smit TS. The use of a quadruped as an in vivo model for the study of the spine - biomechanical considerations. Eur Spine J 2002;11:137–44. https://doi.org/10.1007/s005860100346.
[39] Wolff J. Uber die Innere Architektur der Knochen unk ihre Bedeutung fur die Frage vom Knochenwachstum. Arch Pathol, Anat Physiol Klin Virchows Arch. 1870;50:389–453.
[40] Turner CH. On Wolff's law of trabecular architecture. J Biomech 1992;25:1–9. https://doi.org/10.1016/0021-9290(92)90240-2.
[41] Wang J, Ishimoto T, Nakano T. Unloading-induced degradation of the anisotropic arrangement of collagen/apatite in rat femurs. Calcif Tissue Int 2017;100:87–97. https://doi.org/10.1007/s00223-016-0200-0.
[42] Burger EH, Klein-Nulend J. Mechanotransduction in bone - role of the lacuno-canalicular network. FASEB J 1999;13:S101–12. https://doi.org/10.1096/fasebj.13.9001.s101.
[43] Bonewald LF. The amazing osteocyte. J Bone Miner Res 2011;26:229–38. https://doi.org/10.1002/jbmr.320.
[44] Ishimoto T, Kawahara K, Matsugaki A, Kamioka H, Nakano T. Quantitative evaluation of osteocyte morphology and bone anisotropic extracellular matrix in rat femur. Calcif Tissue Int 2021;109:434–44. https://doi.org/10.1007/s00223-021-00852-1.
[45] Li H, Zou X, Xue Q, Egund N, Lind M, Bünger C. Effects of autogenous bone graft impaction and tricalcium phosphate on anterior interbody fusion in the porcine lumbar spine. Acta Orthop Scand 2004;75:456–63. https://doi.org/10.1080/00016470410001240-1.
[46] Takahashi H, Ishimoto T, Inoue T, Kimura H, Uetsuki K, Okuda N, et al. Effects of autogenous bone graft on mass and quality of trabecular bone in Ti-6Al-4V spinal cage fabricated with electron beam melting. Mater Trans 2019;60:144–8. https://doi.org/10.2320/matertrans.M2018329.
[47] D'Souza M, Macdonald NA, Gendreau JL, Duddleston PJ, Feng AY, Ho AL. Graft materials and biologics for spinal interbody fusion. Biomedicines 2019;7:75. https://doi.org/10.3390/biomedicines7040075.
[48] Kumara P, Prakash O, Ramamurty U. Micro-and meso-structures and their influence on mechanical properties of selectively laser melted Ti-6Al-4V. Acta Mater 2018;154:246–60. https://doi.org/10.1016/j.actamat.2018.05.044.
[49] Laratta JL, Vivace BJ, López-Peña M, Guzón FM, Gonzalez-Cantalpeidra A, Jorge-Mora A, et al. 3D-printed titanium cages without bone graft outperform PEEK cages with autograft in an animal model. Spine J 2022;22:1016–27 in press. https://doi.org/10.1016/j.spinee.2021.12.004.
[50] Heary RF, Parvathreddy N, Sampath S, Agarwal N. Elastic modulus in the selection of interbody implants. J Spine Surg 2017;3:163–7. https://doi.org/10.21037/jss.2017.05.01.
[51] Ishimoto T, Hagihara K, Hisamoto K, Sun SH, Nakano T. Crystallographic texture control of beta-type Ti-15Mo-5Zr-3Al alloy by selective laser melting for the development of novel implants with a biocompatible low Young's modulus. Scr Mater 2017;132:34–8. https://doi.org/10.1016/j.scriptamat.2016.12.038.
[52] Lee SH, Todai M, Tane M, Hagihara K, Nakajima H, Nakano T. Biocompatible low Young's modulus achieved by strong crystallographic elastic anisotropy in Ti-15Mo-5Zr-3Al alloy single crystal. J Mech Behav Biomed Mater 2012;14:48–54. https://doi.org/10.1016/j.jmbbm.2012.05.005.